Research Article | DOI:10.5281/zenodo.10403119
www.jnanosam.com

NANOSAM
Journal of NanoScience in Advanced Materials

Modelling the Magnetocaloric Effect Arising from critical Behavior of Tb_2Rh_3Ge Rare-Earth

Salha Khadhraoui[1#], Nadia Zaidi[2] and Hanen Hammemi[1]

In this paper, we investigated the critical behavior during the transition from the ferromagnetic to paramagnetic phase in Tb_2Rh_3Ge rare-earth. Utilizing the Landau theory, we produced isothermal magnetization curves, *M*(*H,T*), in the vicinity of the ferromagnetic-to-paramagnetic phase transition. Through an iterative program utilizing the Kouvel-Fisher method, we determined the optimized critical exponents to be: γ=1.003; β=0.348. These critical exponents are clear and reasonably consistent, although they do not align with the conventional universality classes. We have successfully simulated the magnetic entropy change curves by combining the Arrott-Noakes equation with the Landau model.

1. Introduction

Changes in physical properties during the ferromagnetic-to-paramagnetic phase transition play a crucial role in the functionalities and underlying physics of magnetic materials, with a broad spectrum of applications. These applications include magnetic sensors [1], magnetic storage devices [2, 3], spintronics devices [4] and magnetic cooling [5], among others. Notably, magnetic refrigeration relies on the magnetocaloric effect (MCE), which results in a reversible temperature change in a material when exposed to varying magnetic fields [6]. An enhanced magnetic cooling system could achieve up to 60% Carnot efficiency, providing greater energy efficiency and cost-effectiveness [7]. Furthermore, it offers compactness, a more environmentally friendly footprint, and a quieter operating environment due to the use of a magnetic solid instead of traditional refrigerant fluids.

The character of a magnetic transition significantly influences the practical applications of these materials. Two fundamental inquiries regarding this phase transition include determining the transition's order and establishing its universality class based on the critical behavior.

Regarding critical behavior, various measurable parameters in the vicinity of the paramagnetic-to-ferromagnetic phase transition can be described by power laws defined through critical exponents [8, 9]. These exponent values help classify magnetic alloys and elucidate their behavior [10, 11]. Within the category of second-order magnetic materials, rare-earth-based intermetallic compounds are notable for their dense structures and the presence of significant, localized magnetic moments [12]. Intermetallic alloys, owing to their diverse applications, represent a valuable source for the development of MCE materials with potential benefits [13, 14]. They are recognized for their high total magnetic moment quantum number J, primarily due to the presence of rare earth elements. Additionally, the Lande factor g contributes to the amplification of the magnetothermal effect in these materials [13]. Furthermore, they can be categorized into three groups for refrigeration applications based on their operational temperature range, typically in proximity to the transition temperature [15]. The initial category encompasses temperatures below 80 K, such as $Gd_{20}Ho_{20}Tm_{20}Cu_{20}Ni_{20}$ [16], $Er_{20}Ho_{20}Gd_{20}Ni_{20}Co_{20}$ [17] and RE_6Co_2Ga [18]. The second group falls within the range of moderate temperatures, specifically between 80 and 250 K, such as DyZn [19] and $La_{1-x}Pr_xFe_{12}B_6$ [20]. The third category encompasses temperatures found in typical room conditions (higher than 250 K), such as the nonstoichiometric $Er_{0.65}Gd_{0.35}Co_2Mn_x$ compounds [21]. Recently, Sahu and Strydom [12]

[1]AL-Baha University, Faculty of Science, Department of Physics, 65779, Al Bahah, Saudi Arabia, [2]Jouf University, College of Sciences, Department of Physics, 72388, Aljouf, Saudi Arabia.
#Corresponding author: salhakhadhraoui@gmail.com

Keywords: Magnetizations; Critical behavior; Landau model; Spontaneous magnetization; Modified Arrott plot.

Received: 24 October 2023 | Accepted: 06 November 2023 | Published: 22 December 2023

NANOSAM
Journal of NanoScience in Advanced Materials

provided details on the crystal structure, magnetic properties, and MCE in Tb_2Rh_3Ge compound. The polycrystalline Tb_2Rh_3Ge sample was synthesized using the arc-melting technique. The Tb_2Rh_3Ge alloy was crystallized in Mg_2Ni_3Si-type of rhombohedral Laves phases. Isothermal magnetizations were measured at different temperatures T around T_C=56 K.

In the context of modeling, theoretical approaches [22-25] result in the simulation of isotherms M(H,T). Efficient numerical techniques can be utilized to streamline data generation without relying on expensive and time-consuming experimental measurements. Employing numerical methods [22-25] enables the resolution of the transcendental equation to ascertain isothermal magnetization. The efficacy of these theoretical approaches can streamline and minimize the need for numerous experimental measurements. In this work, we have described the critical behavior of Tb2Rh3Ge rare-earth after generating isotherms M(H,T) curves around the Curie temperature T_C based on the Landau theory. By employing an iterative method on a modified Arrot plot (MAP) [26] the critical exponents β, γ are set and deduced again from the spontaneous magnetization vs. temperature, M_S(T), and the inverse of the magnetic susceptibility vs. temperature, $\chi_0^{-1}(T)$, curves. Therefore, we examined an efficient approach centered on the analysis of Gibbs free energy using the Landau model. Based on this resilient Landau model, $-\Delta S_M$ curves could be simulated over a broad range of validity, making this method a strong contender among promising theoretical models for MCE simulations.

2. Results and Discussion

2.1. Arrott–Noakes equation

Near a second-order paramagnetic to ferromagnetic phase transition in a magnetic material, the Arrott-Noakes equation of state (ANE) is expressed, considering the critical exponents β and γ [27]:

$$\left(\frac{H}{M}\right)^{\frac{1}{\gamma}} = a_0(T - T_C) + b_0 M^{\frac{1}{\beta}} \tag{1}$$

where a_0 and b_0 are constants. The scaling relations of Eq. (1) set the spontaneous magnetization and the inverse initial magnetic susceptibility $\chi_0{}^{-1}$as function as the reduced temperature $\varepsilon = \frac{T - T_C}{T}$ [28]:

$$M_S = M_0(-\varepsilon)^{\beta}\ ;\ T < T_C, \tag{2}$$

$$\chi_0{}^{-1} = h_0 \varepsilon^{\gamma}\ ;\ T > T_C, \tag{3}$$

with M_0, h_0 and X_0 are critical amplitudes.

Indeed, the utilization of the ANE is applicable within an extremely limited range: $|\varepsilon| < 0.1$ [29]. The concerning temperatures, from given M(H, T) data, giving $|\varepsilon| < 0.1$ are: 52, 54, 56, 58 and 60 K. Consequently, these limited isotherms around T_C are not suitable for categorizing theM_S(T) and $\chi_0{}^{-1}$(T). Hence, we turn to the Landau theory to produce additional isotherms M(H, T) from 52 to 60 K region.

2.2. Landau theory

In the vicinity of the T_C, the Landau expansion of the Gibbs free energy, G, is given as [30]:

$$G(T, M) \cong G_0 + \frac{1}{2}A(T)M^2 + \frac{1}{4}B(T)M^4 + \frac{1}{6}C(T)M^6 - MH, \tag{4}$$

where the constant G_0 is the energy reference, the parameters $A(T)$, $B(T)$, and $C(T)$ are temperature-dependent variables that characterize magnetoelastic coupling and electron condensation energy.

By applying the state of equilibrium near T_C, $\frac{\partial G}{\partial M} = 0$, the magnetic state equation is derived as follows:

$$\frac{H}{M} = A(T) + B(T)M^2 + C(T)M^4 \tag{5}$$

The A(T), B(T) and C(T) parameters can be calculated from the quadratic fitting of $\frac{H}{M}$ vs. M^2 based on Eq. (5). Figure 1 presents the A(T), B(T) and C(T) coefficients which can be fitted by polynomial fits.

Subsequently, solving Eq. (5) with MATLAB software could yield isotherms M(H, T) at any temperature in $|\varepsilon| < 0.1$-region. Generated M(H, T) from 52 to 60 K with 0.5 K temperature step were depicted in Figure 2.

2.3. Critical behavior analysis

The appropriate values for β and γ are fine-tuned to ensure the generation of modified Arrot plots (MAP). $M^{\frac{1}{\beta}}$ vs. $\left(\frac{H}{M}\right)^{\frac{1}{\gamma}}$, that exhibit parallel linear patterns. Additionally, the critical isotherm (at T = T_C). The critical isotherm should manifest as a linear curve originating from the origin. Choosing suitable values for the exponents γ and β can be challenging, as incorporating these two adjustable parameters in Eq. (1) may result in non-physical fits and systematic errors in exponent values. To address this challenge, an iterative program based on the Kouvel-Fisher method [31] was implemented to sort out the proper γ and β values. Initially, arbitrary values for γ and β were selected. The program in place will iteratively adjust these values until two specific conditions are met: (i) Isotherms

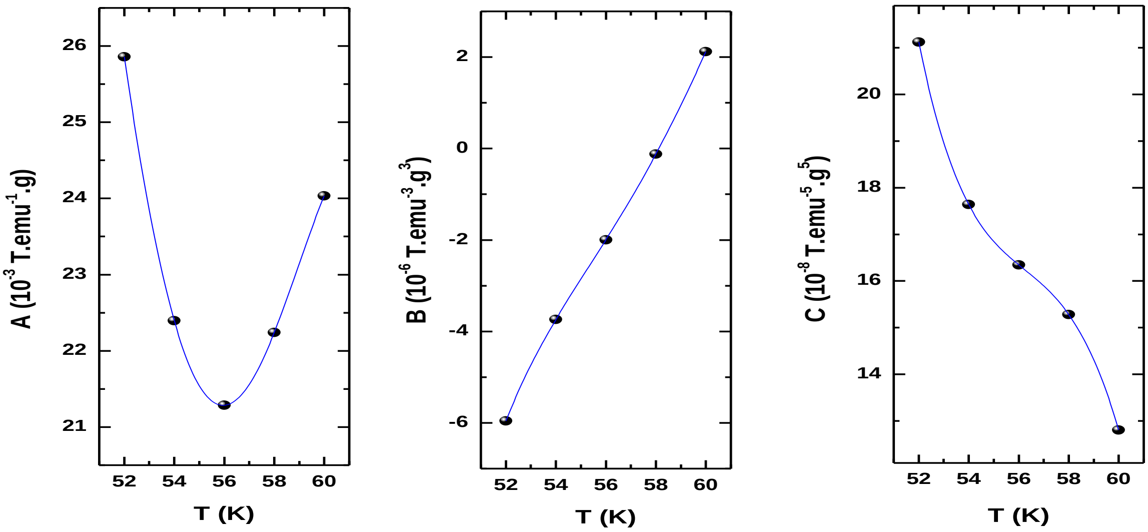

Figure 1. The temperature-dependent coefficients A(T), B(T) and C(T) near T_C for Tb_2Rh_3Ge sample.

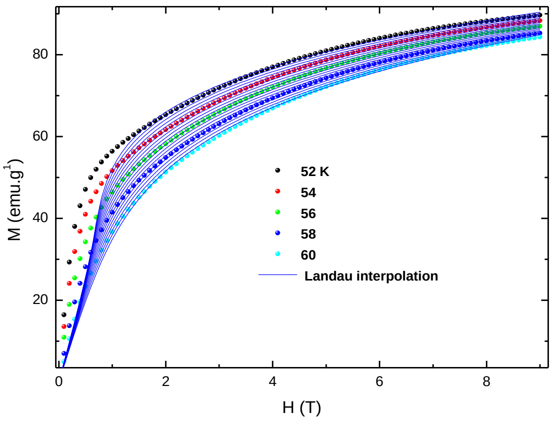

Figure 2. Interpolating M(H, T) from 52 to 60 K with 0.5 K temperature using Landau model for Tb_2Rh_3Ge.

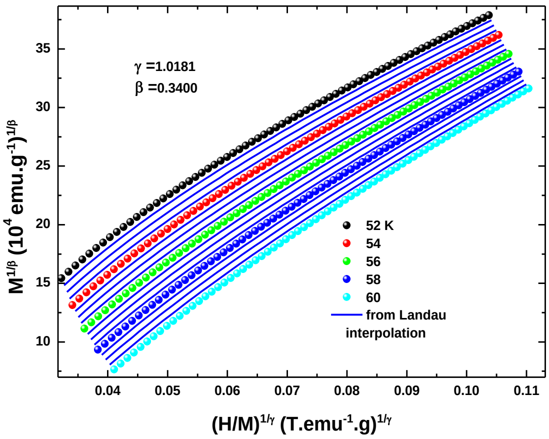

Figure 3. Modified Arrot plots (MAP), $M^{\frac{1}{\beta}}$ vs. $\left(\frac{H}{M}\right)^{\frac{1}{\gamma}}$, for the Tb_2Rh_3Ge alloy.

$M^{\frac{1}{\beta}}$ vs. $\left(\frac{H}{M}\right)^{\frac{1}{\gamma}}$ form straight lines that are parallel, and (ii) the critical isotherm (at $T = T_C$) intersects at the starting point.

The values that remained stable were identified as: $\gamma = 1.0181$ and $\beta = 0.3400$ for Tb_2Rh_3Ge. These values were used to create a group of straight lines which are clearly parallel in Figure 3.

In Figure 3, it is worth noting that the linear fits of the MAP only encompass the higher magnetic field regions, as at lower field strengths, the isotherms become magnetized and align in various directions [32].

The linear regressions of the MAP provide $M_S^{1/\beta}$ and $(\chi_0{}^{-1})^{1/\gamma}$. The $M_S(T)$ and $\chi_0{}^{-1}(T)$ results for Tb_2Rh_3Ge are represented in Figure 4. Fitting $M_S(T)$ using Eq. (2) gives: $\beta = 0.360$; $T_C = 56.044$ K and $M_0 = 126.735$ $\mathrm{emu.g^{-1}}$. Nevertheless, fitting $\chi_0{}^{-1}(T)$ using Eq. (3) provides: $\gamma = 1.003$; $T_C = 55.999$ K and $h_0 = 0.229$ $\mathrm{T.emu^{-1}.g}$.

For a more precise determination of the critical exponents, utilizing a Log-Log scale on Eq. (2) and Eq. (3) results in: $\ln\left(\frac{M_S}{M_0}\right) = \beta \log(-\varepsilon)$ and $\ln\left(\frac{\chi_0{}^{-1}}{h_0}\right) = \gamma \log(\varepsilon)$. The linear regressions of the: $\ln\left(\frac{M_S}{M_0}\right)$ vs. $\ln(-\varepsilon)$ and $\log\left(\frac{\chi_0{}^{-1}}{h_0}\right)$ vs. $\ln(\varepsilon)$ give $\beta = 0.348$ and $\gamma = 1.003$ as indicated in Figure 5.

Observing Figure 5, it becomes evident that β value is more similar to the one optimized using the iterative approach ($\beta = 0.348$).

These critical exponents (γ and β) do not align with the traditional universality classes: Mean - Field, 3D Heisenberg, 3D Ising, Tricritical Mean - Field Models.

To reaffirm the reliability of the obtained critical exponent values, additional assurance can be obtained through a more effective method involving scaling plots $M|\varepsilon|^{-\beta}$ vs. $H|\varepsilon|^{-(\beta+\gamma)}$ as shown in Figure 6.

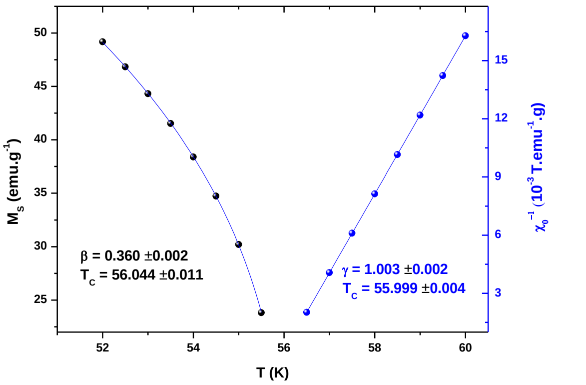

Figure 4. Fitting $M_S(T)$ and $\chi_0{}^{-1}(T)$, with Eq. (2) and Eq. (3), respectively, for Tb_2Rh_3Ge compound.

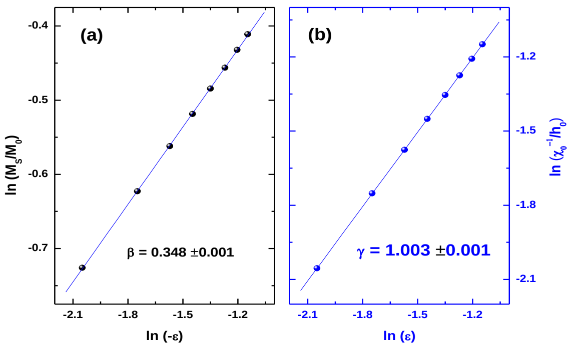

Figure 5. The linear fit of **(a)** $\ln\left(\frac{M_S}{M_0}\right)$ vs. $\log(-\varepsilon)$ and **(b)** of $\ln\left(\frac{\chi_0{}^{-1}}{h_0}\right)$ vs. $\log(\varepsilon)$ for Tb_2Rh_3Ge.

To reaffirm the reliability of the obtained critical exponent values, additional assurance can be obtained through a more effective method involving scaling plots: one above T_C and another below T_C. This affirms the unambiguous and reasonable nature of the critical exponents.

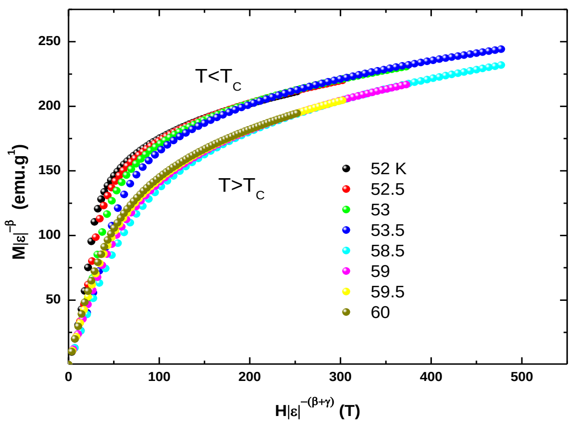

Figure 6: The scaling plots $M|\varepsilon|^{-\beta}$ vs. $H|\varepsilon|^{-(\beta+\gamma)}$ below and above T_C.

2.4. Critical exponents and Landau models

The expression for the Gibbs free energy in a disordered ferromagnetic system undergoing a second-order phase transition can be formulated using the Landau model as follows [29]:

$$G(T,M) = G_0 + \left[\frac{1}{\frac{1}{\gamma}+1} a(T) M^{\frac{1}{\gamma}+1} + \frac{1}{\frac{1}{\beta}+\frac{1}{\gamma}+1} b(T) M^{\frac{1}{\beta}+\frac{1}{\gamma}+1} - M H^{\frac{1}{\gamma}}\right] H^{1-\frac{1}{\gamma}} \quad (6)$$

where G_0 is the reference energy, a(T) and b(T) the temperature-dependent parameters encompass the magnetoelastic coupling and the energy associated with electron condensation [33]. The condition for minimizing Eq. (6), $\left(\frac{dG}{dM}\right)_T = 0$, leads to:

$$\left(\frac{H}{M}\right)^{\frac{1}{\gamma}} = a(T) + b(T) M^{\frac{1}{\beta}} \quad (7)$$

However, the magnetic entropy $\left(S_M = -\frac{dG}{dT}\right)$ by removing the spontaneous magnetization [34] could be formulated as:

$$-\Delta S_M = \left[\frac{1}{\frac{1}{\gamma}+1}\frac{dA(T)}{dT}\left(M^{\frac{1}{\gamma}+1} - M_S{}^{\frac{1}{\gamma}+1}\right) + \frac{1}{\frac{1}{\beta}+\frac{1}{\gamma}+1}\frac{dB(T)}{dT}\left(M^{\frac{1}{\beta}+\frac{1}{\gamma}+1} - M_S{}^{\frac{1}{\beta}+\frac{1}{\gamma}+1}\right)\right] H^{1-\frac{1}{\gamma}} \quad (8)$$

Magnetizations M vs. applied magnetic field H, at different temperatures from 40 to 70 K with 2 K temperature step [21] are shown in Figure 7(a). With the dependable γ and β values estimated above, isotherms $\left(\frac{H}{M}\right)^{\frac{1}{\gamma}}$ vs. $M^{\frac{1}{\beta}}$ within the temperature range for holes and in the presence of strong magnetic fields for the Tb_2Rh_3Ge compound are graphed in Figure 7(b).

In accordance with the expression given in Eq. (7), linear regression analysis of $\left(\frac{H}{M}\right)^{\frac{1}{\gamma}}$ vs. $M^{\frac{1}{\beta}}$ give the a(T), b(T) values which are shown in Figure 8 for Tb_2Rh_3Ge sample.

Figure 8 shows these criteria: At $T = T_C, A(T_C) = 0$; $\left.\frac{\partial A}{\partial T}\right|_{T_C} \neq 0$; $B(T_C) \neq 0$ and $\left.\frac{\partial B}{\partial T}\right|_{T_C} = 0$. These criteria align with a second-order ferromagnetic to paramagnetic phase transition, as previously reported by Amaral et al. [29].

NANOSAM
Journal of NanoScience in Advanced Materials

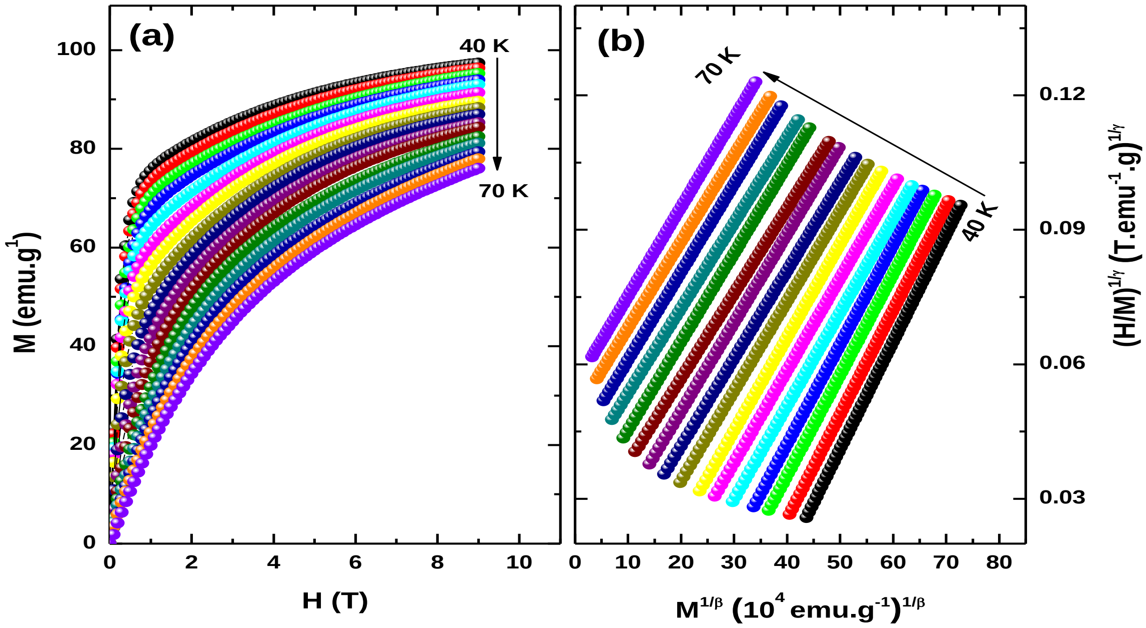

Figure 7. (a) Magnetization M vs. applied magnetic field H, measured at different temperatures from 40 to 70 K with 2 K temperature step [21] and **(b)** the corresponding $\left(\frac{H}{M}\right)^{\frac{1}{\gamma}}$ vs. $M^{\frac{1}{\beta}}$ under high fields (from 2 to 9 T) for Tb_2Rh_3Ge compound.

Solving Eq. (6) with the temperature-dependent parameters $A(T)$ and $B(T)$ results in the generation of isotherms for M. The generated M and the calculated M_S with the γ and β values are inserted in Eq. (7) to generate $-\Delta S_M(T)$ curves. These $-\Delta S_M(T)$ curves (blue lines) in Figure 9 are presented and juxtaposed with the respective experimental data points (symbols) for the Tb_2Rh_3Ge alloy.

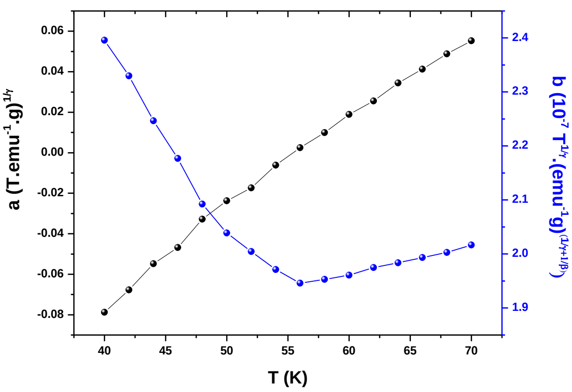

Figure 8. The changes in temperature-dependent parameters a(T)and b(T) near T_C for Tb_2Rh_3Ge sample.

A strong correlation between the computed and experimental strong correlation between the computed and experimental $-\Delta S_M(T)$ curves was observed over a wide temperature range, demonstrating the potential of these theoretical models for simulating the MCE in Tb_2Rh_3Ge alloy.

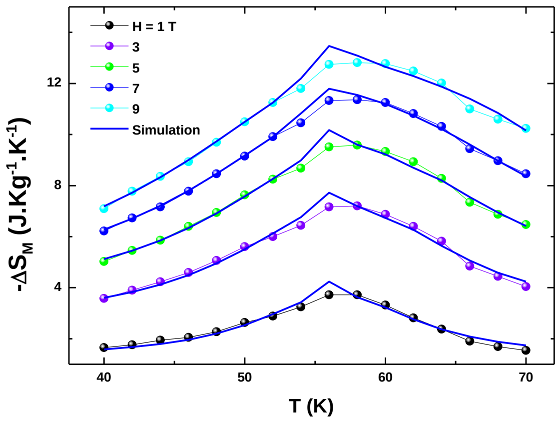

Figure 9. Simulating $-\Delta S_M(T)$ curves (blue lines) under various magnetic fields values using the Landau model. The corresponding experimental results are presented with symbols Tb_2Rh_3Ge

3. Conclusion

Critical behavior at the ferromagnetic paramagnetic phase transition in Tb_2Rh_3Ge alloy was investigated. The Landau theory was used to produce additional isotherms M(H, T) near the ferromagnetic-paramagnetic phase transition of Tb_2Rh_3Ge sample. The exponents (γ ; β) was fine-tuned to (1.003;0.348). Utilizing these critical exponent values, an examination of the Landau model was carried out by employing the Gibbs free energy. Subsequently, the Landau model was successful in simulating$-\Delta S_M(H,T)$ curves.

Authors' contributions:

The manuscript was written with the contributions of all authors. SK contributed to preparing data. ND contributed to editing of the manuscript. HH contributed to calculations.

Data Availability Statement

Data are available upon request.

References

[1] Abdel-Latif, I.A., Hassen, A., Zybill, C., Abdel-Hafiez, M., Allam, S., and El-Sherbini, T. "The influence of tilt angle on the CMR in Sm0.6Sr0.4MnO3", Journal of Alloys and Compounds **452** (2) 245-248 (2008).

[2] Bally, M.A.A. and Khan, F.A. "Structural, dielectric and magnetic properties of La0.55Sr0.45MnO3 polycrystalline perovskite", Journal of Magnetism and Magnetic Materials **509** 166897 (2020).

[3] Xia, W., Pei, Z., Leng, K., and Zhu, X. "Research Progress in Rare Earth-Doped Perovskite Manganite Oxide Nanostructures", Nanoscale Research Letters **15** (1) 9 (2020).

[4] EGILMEZ, M., CHOW, K.H., and JUNG, J.A. "ANISOTROPIC MAGNETORESISTANCE IN PEROVSKITE MANGANITES", Modern Physics Letters B **25** (10) 697-722 (2011).

[5] Al-Yahmadi, I.Z., Gismelseed, A.M., Al Ma'Mari, F., Al-Rawas, A.D., Al-Harthi, S.H., Yousif, A.Y., Widatallah, H.M., Elzain, M.E., and Myint, M.T.Z. "Structural, magnetic and magnetocaloric effect studies of Nd0.6Sr0.4AxMn1-xO3 (A=Co, Ni, Zn) perovskite manganites", Journal of Alloys and Compounds **875** 159977 (2021).

[6] Lyubina, J. "Magnetocaloric materials for energy efficient cooling", Journal of Physics D: Applied Physics **50** (5) 053002 (2017).

[7] Zimm, C., Jastrab, A., Sternberg, A., Pecharsky, V., Gschneidner, K., Osborne, M., and Anderson, I., *Description and Performance of a Near-Room Temperature Magnetic Refrigerator*, in *Advances in Cryogenic Engineering*, P. Kittel, Editor Springer US: Boston, MA. p. 1759-1766 (1998)

[8] Li, Y., Feng, S., Lv, Q., Kan, X., and Liu, X. "An investigation of reentrant spin-glass behavior, magnetocaloric effect and critical behavior of MnCr2O4", Journal of Alloys and Compounds **877** 160224 (2021).

[9] Ahmed, A., Mazumdar, D., Das, K., and Das, I. "A comparative study of the magnetic and magnetocaloric effect of polycrystalline Gd0.9Y0.1MnO3 and Gd0.7Y0.3MnO3 compounds: Influence of Y-ions on the magnetic state of GdMnO3", Journal of Magnetism and Magnetic Materials **551** 169133 (2022).

[10] Ma, S.-K., *Modern theory of critical phenomena*. Reading,(MA). London: Addison-Wesley (1976)

[11] Huang, K., *Statistical Mechanics*. New York: Wiley (1987)

[12] Sahu, B. and Strydom, A.M. "Magnetic properties and magnetocaloric effect of Tb2Rh3Ge", Journal of Magnetism and Magnetic Materials **541** 168444 (2022).

[13] Chen, H., Zhang, Y., Han, J., Du, H., Wang, C., and Yang, Y. "Magnetocaloric effect in R2Fe17 (R=Sm, Gd, Tb, Dy, Er)", Journal of Magnetism and Magnetic Materials **320** (7) 1382-1384 (2008).

[14] Li, L., Xu, P., Ye, S., Li, Y., Liu, G., Huo, D., and Yan, M. "Magnetic properties and excellent cryogenic magnetocaloric performances in B-site ordered RE2ZnMnO6 (RE = Gd, Dy and Ho) perovskites", Acta Materialia **194** 354-365 (2020).

[15] Huang, G.B., Du, Y.S., Wu, X.F., Ma, L., Li, L., Cheng, G., Wang, J., Zhao, J.T., and Rao, G.H. "Tunable magnetocaloric effect at approximately room temperature by Y-substitution in Ho2Fe17", Intermetallics **143** 107487 (2022).

[16] Zhang, Y., Wu, B., Guo, D., Wang, J., and Ren, Z. "Magnetic properties and promising cryogenic magneto-caloric performances of Gd20Ho20Tm20Cu20Ni20 amorphous ribbons*", Chinese Physics B **30** (1) 017501 (2021).

[17] Yikun Zhang, Jian Zhu, Shuo Li, Wang, J., and Ren, Z. "Achievement of giant cryogenic refrigerant capacity in quinary rare-earths based high-entropy amorphous alloy", J. Mater. Sci. Technol. **102** 66-71 (2022).

[18] Guo, D., Moreno-Ramírez, L.M., Romero-Muñiz, C., Zhang, Y., Law, J.-Y., Franco, V., Wang, J., and Ren, Z. "First- and second-order phase transitions in RE6Co2Ga (RE = Ho, Dy or Gd) cryogenic magnetocaloric materials", Science China Materials **64** (11) 2846-2857 (2021).

[19] Wang, X.-J., Wang, L., Ma, Q., Sun, G., Zhang, Y., and Cui, J.-z. "Magnetic phase transitions and large magnetocaloric effects in equiatomic binary DyZn compound", Journal of Alloys and Compounds **694** 613-616 (2017).

[20] Ma, Z., Dong, X., Zhang, Z., and Li, L. "Achievement of promising cryogenic magnetocaloric performances in La1-xPrxFe12B6 compounds", Journal of Materials Science & Technology **92** 138-142 (2021).

[21] Gerasimov, E.G., Inishev, A.A., Mushnikov, N.V., Terentev, P.B., Gaviko, V.S., and Anikin, M.S. "Magnetocaloric effect, heat capacity and exchange interactions in nonstoichiometric Er0.65Gd0.35Co2Mnx compounds", Intermetallics **140** 107386 (2022).

[22] Erchidi Elyacoubi, A.S., Masrour, R., and Jabar, A. "Magnetocaloric effect and magnetic properties in SmFe1-xMnxO3 perovskite: Monte Carlo simulations", Solid State Communications **271** 39-43 (2018).

[23] van Dijk, N.H. "Landau model evaluation of the magnetic entropy change in magnetocaloric materials", Journal of Magnetism and Magnetic Materials **529** 167871 (2021).

[24] Hsini, M., Hcini, S., and Zemni, S. "Magnetocaloric effect studying by means of theoretical models in Pr0.5Sr0.5MnO3 manganite", Journal of Magnetism and Magnetic Materials **466** 368-375 (2018).

[25] Hsini, M., Hcini, S., and Zemni, S. "Magnetocaloric effect simulation by Landau theory and mean-field approximation in Pr0.5Sr0.5MnO3", The European Physical Journal Plus **134** (12) 588 (2019).

[26] Pramanik, A.K. and Banerjee, A. "Critical behavior at paramagnetic to ferromagnetic phase transition in

${\text{Pr}}_{0.5}{\text{Sr}}_{0.5}{\text{MnO}}_{3}$: A bulk magnetization study", Physical Review B **79** (21) 214426 (2009).

[27] Arrott, A. and Noakes, J.E. "Approximate Equation of State For Nickel Near its Critical Temperature", Physical Review Letters **19** (14) 786-789 (1967).

[28] Fisher, M.E. "The theory of equilibrium critical phenomena", Reports on Progress in Physics **30** (2) 615 (1967).

[29] Zhang, L., Fan, J., and Zhang, Y. "Magnetic entropy calculation for a second-order ferromagnetic phase transition", Modern Physics Letters B **28** (08) 1450059 (2014).

[30] Amaral, V.S. and Amaral, J.S. "Magnetoelastic coupling influence on the magnetocaloric effect in ferromagnetic materials", Journal of Magnetism and Magnetic Materials **272-276** 2104-2105 (2004).

[31] Kouvel, J.S. and Fisher, M.E. "Detailed Magnetic Behavior of Nickel Near its Curie Point", Physical Review **136** (6A) A1626-A1632 (1964).

[32] Aharoni, A., *Introduction to the Theory of Ferromagnetism* Clarendon Press: Oxford (1996)

[33] Eremin, I.M., Knolle, J., and Moessner, R., *Magnetism and Superconductivity*, in *Handbook of Magnetism and Magnetic Materials*, M. Coey and S. Parkin, Editors Springer International Publishing: Cham. p. 1-31 (2020)

[34] Dong, Q.-y., Zhang, H.-w., Shen, J.-l., Sun, J.-r., and Shen, B.-g. "Field dependence of the magnetic entropy change in typical materials with a second-order phase transition", Journal of Magnetism and Magnetic Materials **319** (1) 56-59 (2007).